Plasma Modeling and First Wall Interaction Phenomena in Tokamaks

R.W. Conn and J. Kesner

February 1976

UWFDM-153

Published in *Journal of Nuclear Materials 63 (1976) 1-14.*

FUSION TECHNOLOGY INSTITUTE

UNIVERSITY OF WISCONSIN

MADISON WISCONSIN

Plasma Modeling and First Wall Interaction Phenomena in Tokamaks

R.W. Conn and J. Kesner

Fusion Technology Institute
University of Wisconsin
1500 Engineering Drive
Madison, WI 53706

http://fti.neep.wisc.edu

February 1976

UWFDM-153

Published in *Journal of Nuclear Materials 63 (1976) 1-14.*

Plasma Modeling and First Wall Interaction Phenomena in Tokamaks

R. W. Conn

J. Kesner

Fusion Technology Program
Nuclear Engineering Department
University of Wisconsin
Madison, WI 53706

UWFDM-153

Feb. 1976

Also published in J. Nucl. Mat. 63 (1976), 1-14.

Abstract

Fluxes of neutral hydrogenic particles, alpha particles and electromagnetic radiation to the liner or first wall of both two component tokamaks and large ignited tokamak fusion reactors are estimated using space and time dependent models of tokamak plasmas. Data requirements and the effects of uncertainties in the areas of first wall interaction phenomenon and plasma transport coefficients are described.

I. Introduction

The importance of interaction phenomena at the first wall of fusion devices is already well appreciated [1] and these phenomena will assume even greater importance as the plasmas produced in confinement experiments become hotter and as we proceed to build fusion reactors. The purpose of this paper is to discuss the relationship between plasma behavior in tokamak devices and the surface effects that can take place at the first wall. This will be done by presenting some results from plasma modeling codes related to the anticipated performance of near term neutral beam driven two component tokamak devices, such as the Tokamak Fusion Test Reactor (TFTR) [2], and larger plasmas that may be characteristics of full scale reactor systems [3].

The radiation emitted by a thermonuclear plasma can be divided into four major types: charged particles, including hydrogen isotopes, helium, electrons and impurities; neutral atoms resulting from gas recycling at the plasma edge and charge exchange processes; electromagnetic radiation including bremsstrahlung, synchrotron emission, bound-bound or line radiation, and free-bound or recombination radiation; and neutrons.

The three primary effects of first wall interaction phenomena are surface erosion, plasma contamination, and surface heating. Surface erosion and surface heating will have a direct effect on the temperature distribution and stress levels in the first wall and will therefore directly effect the choice of first wall thickness and of coolant flow rates and pressures in reactor systems. Surface erosion in a reactor will also impact on the radioactivity control and cleanup systems for the vacuum pumping and cooling system since some of the eroded material will be radioactive [4].

Table 1

Sputtering Yields of Various Materials for Incident H^+ and D^+ (from Finfgeld [17])

Energy (keV)	Au		Co		W		Mo	
	S(H+)	S(D+)	S(H+)	S(D+)	S(H+)	S(D+)	S(H+)	S(D+)
0.5	0.003	0.0166	-	-	-	-	-	-
1.0	0.008	0.027	0.0006	0.0025	2.4×10^{-4}	7×10^{-4}	0.0017	0.0028
2.0	0.018	0.040	0.001	0.0029	2.4×10^{-4}	-	0.0022	0.0035
3.0	0.020	0.036	0.001	0.0028	3×10^{-4}	9.7×10^{-4}	0.0022	0.0036
5.0	0.020	0.047	0.001	0.0029	3×10^{-4}	1×10^{-3}	0.0024	0.0042
7.0	0.022	0.050	0.00078	0.0023	3×10^{-4}	8.8×10^{-4}	0.0033	0.0048

Table 2

Parameters for a Small Circular Two Component Tokamak

Major Radius, (R)	3m
Plasma Radius, (r_p)	1m
Toroidal Field on Axis, (B_T)	50 kG
Initial Target Plasma	Tritium
Plasma Current (at q(a) = 3), (I_p)	2.8 MA
Neutral Beam Injection Energy	150 keV
Assumed Injector Type	"Positive Ion"
Neutral Beam Injection Power	40 MW
Power in D° 60%	
Power in D_2° 24%	
Power in D_3° 18%	

Table 3

3.52 MeV Alpha Particle Characteristics in the Small Two Component Tokamak

Total Alpha Production Rate (α/s)	4.20×10^{18}
Total Alpha Loss Rate Due to Orbits Extending Outside r_p (α/s)	8.93×10^{17}
Fraction of Alphas Lost (%)	21.0
Fraction of Counterstreaming Alphas Lost (%)	41.9
Average Flux to Wall at r_p ($\alpha/cm^2/s$)*	7.5×10^{11}

* This value can be reduced by moving the first wall further back beyond r_p. However, as the first wall radius increases, so does the overall size of the device.

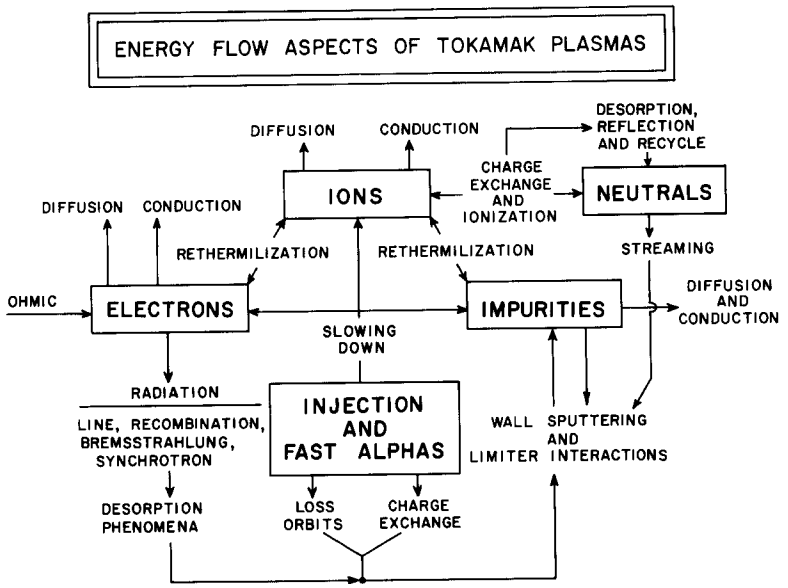

Fig.1 Components of energy flows in tokamaks

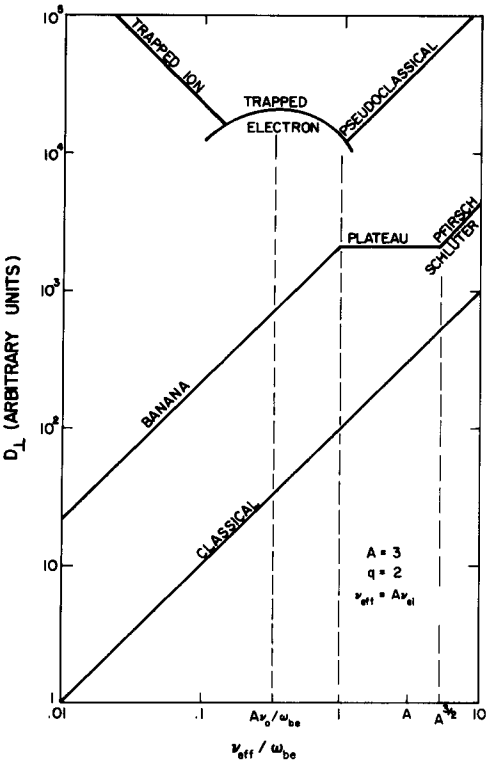

Fig.2 Diffusion coefficients predicted by various theories.

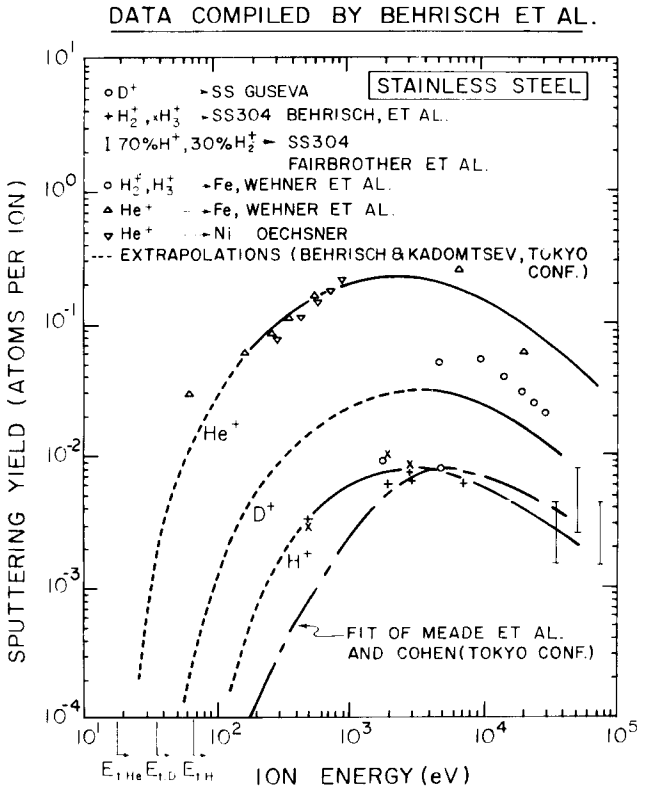

Fig.3 Sputtering yields from stainless steel

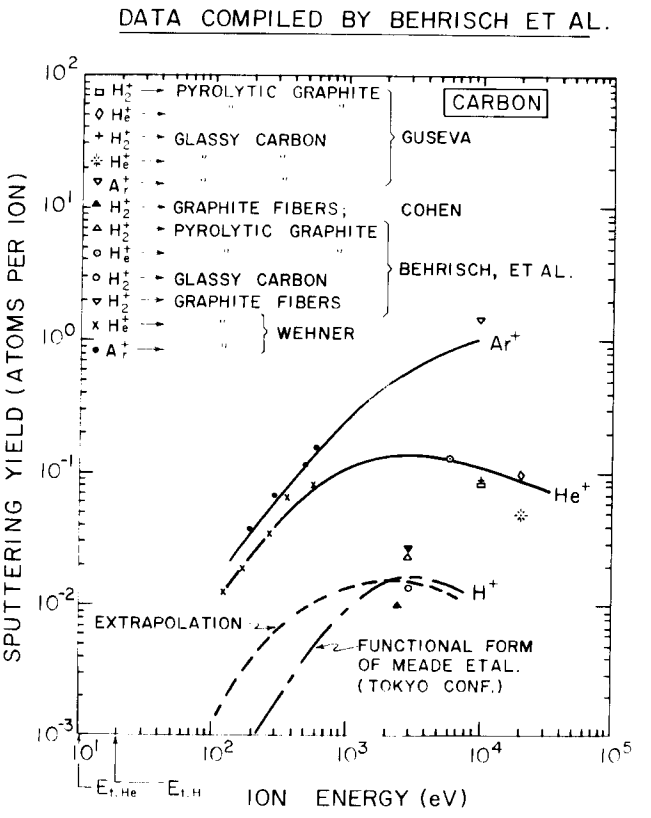

Fig.4 Sputtering yields from carbon.

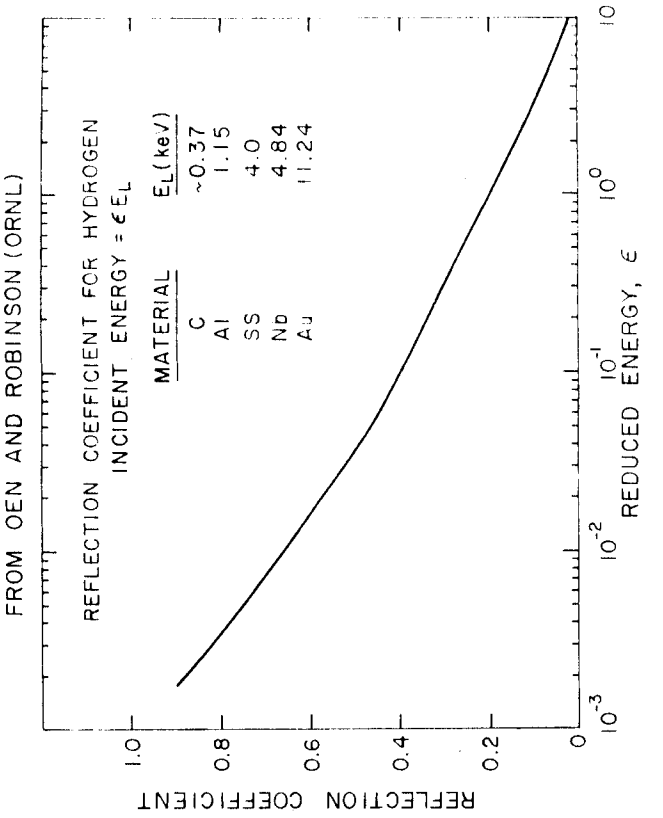

Fig.5 Reflection Coefficient for H versus reduced energy. The Linhard energy, E_L, is given for various materials.

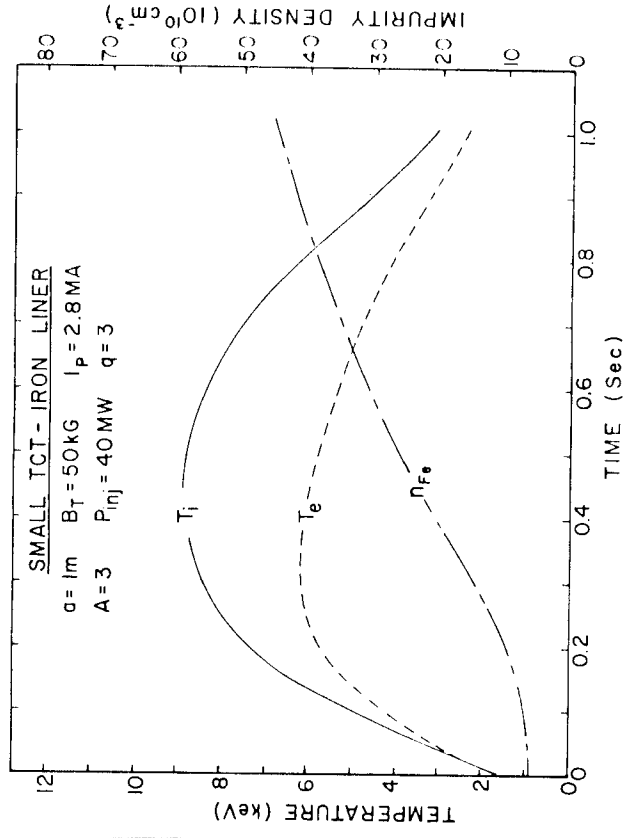

Fig.6 Variation of plasma temperature and impurity content in a TCT. Impurities are assumed to accumulate and initial impurity content is 0.1%.

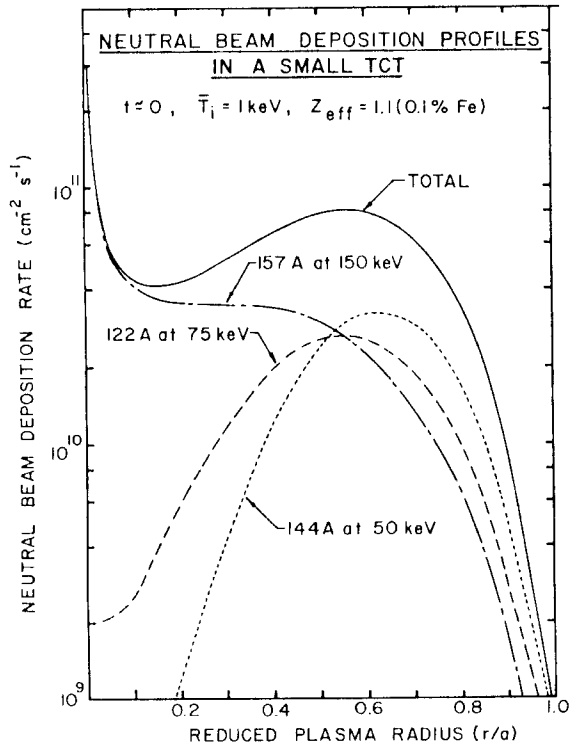

Fig.7 Neutral beam deposition profiles in the small TCT. The low energy components of the beam are attenuated near the plasma edge primarily by charge exchange.

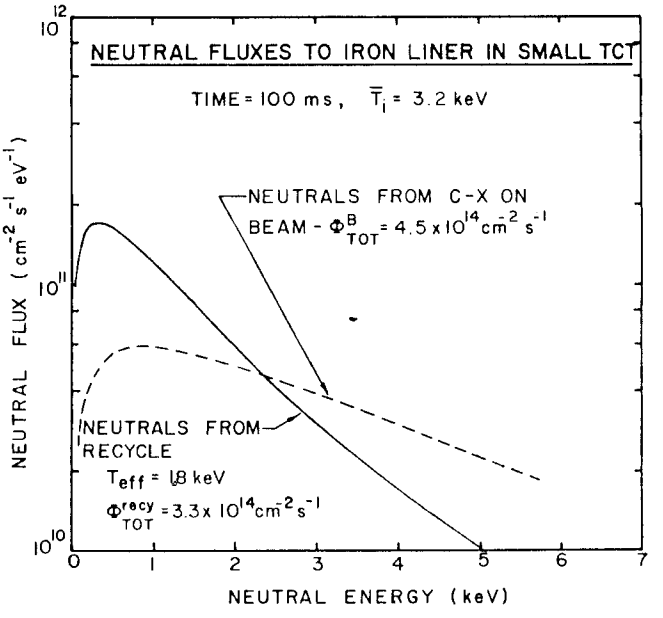

Fig.8 Neutral flux to the liner in the small TCT at t = 100 ms.

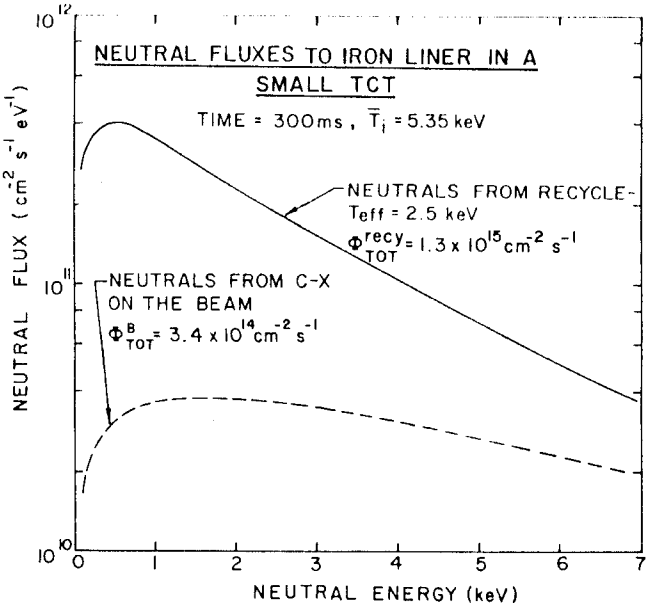

Fig.9 Neutral flux to the liner in the small TCT at t = 300 ms.

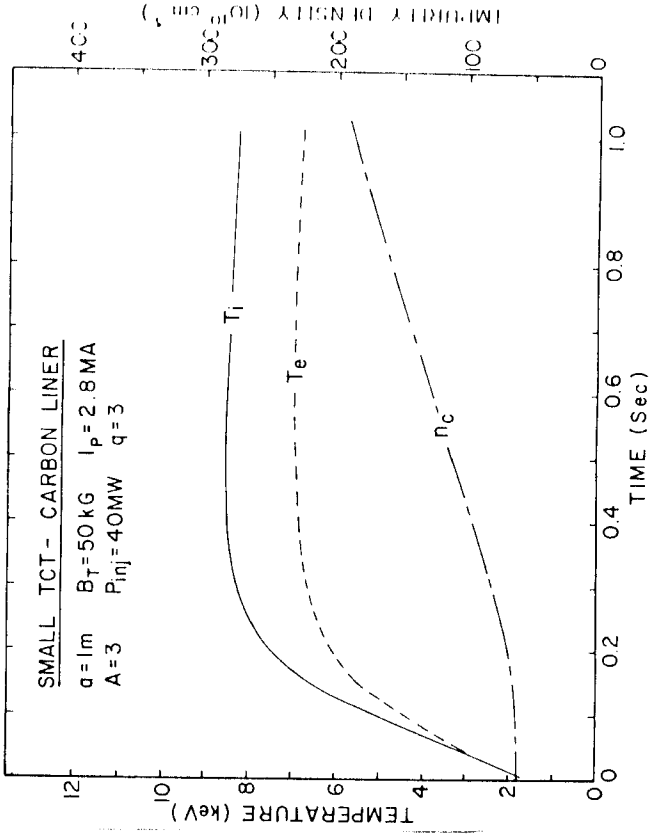

Fig.10 Variation of plasma parameters in the TCT with a carbon liner. Impurities are assumed to accumulate and the initial impurity content is 1%.

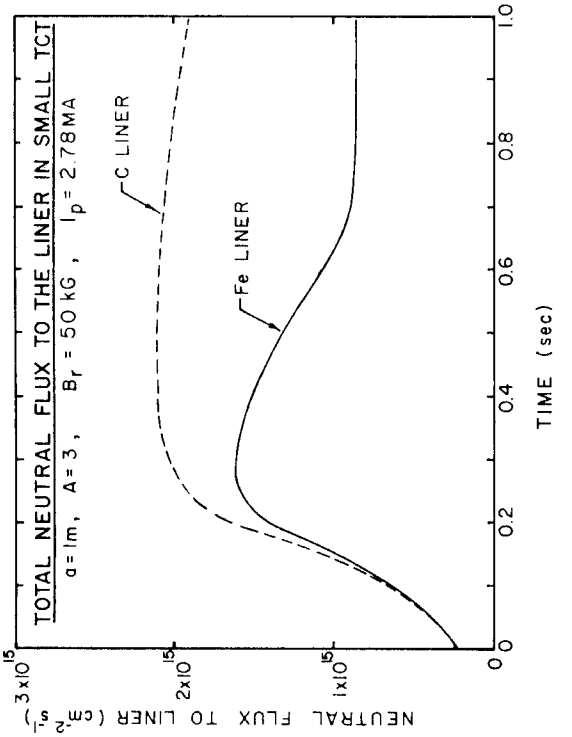

Fig.11 Total flux to the liner in the small TCT as a function of time and the type of liner.

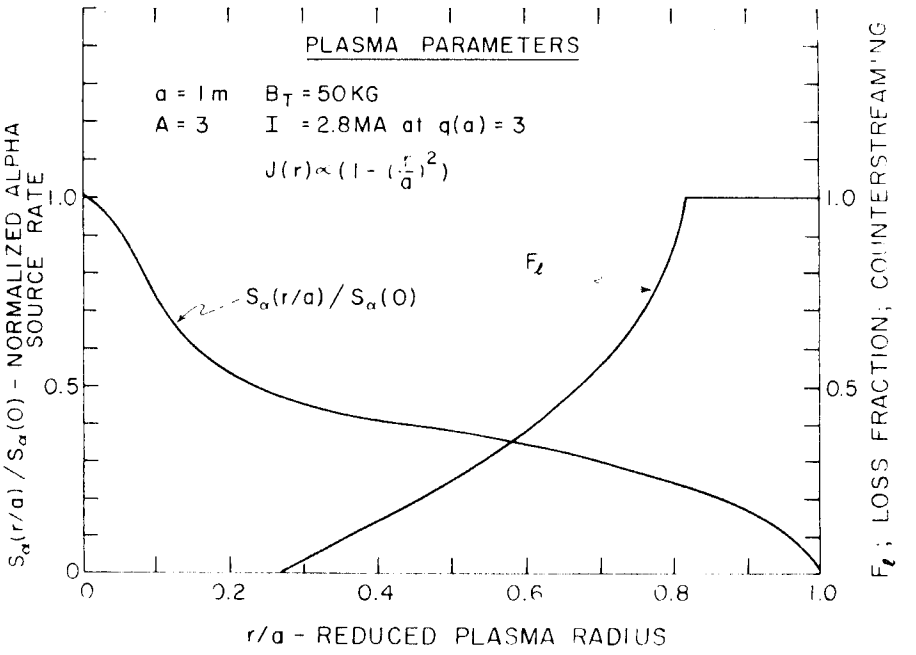

Fig.12 The alpha production profile and the fraction of counterstreaming alphas lost beyond r_p as a function of reduced plasma radius.

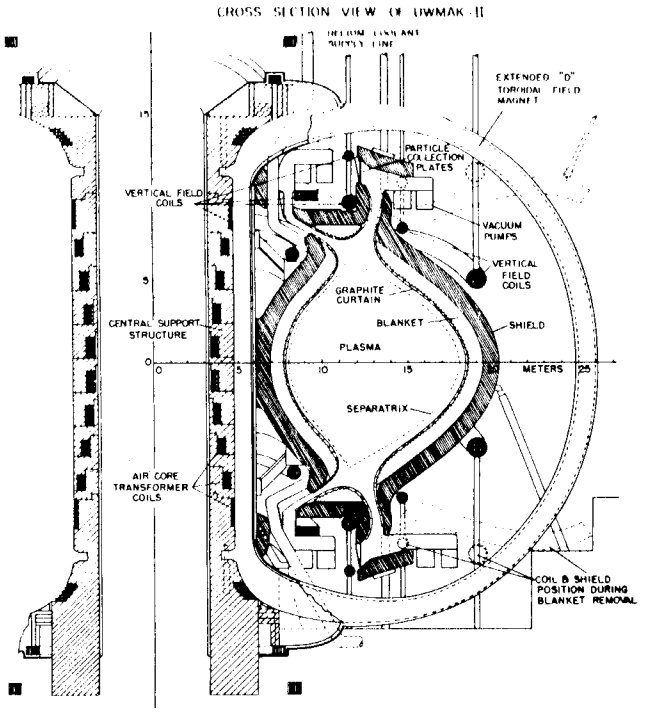

Fig.13 Right half cross section view of the UWMAK-II conceptual tokamak reactor [3].

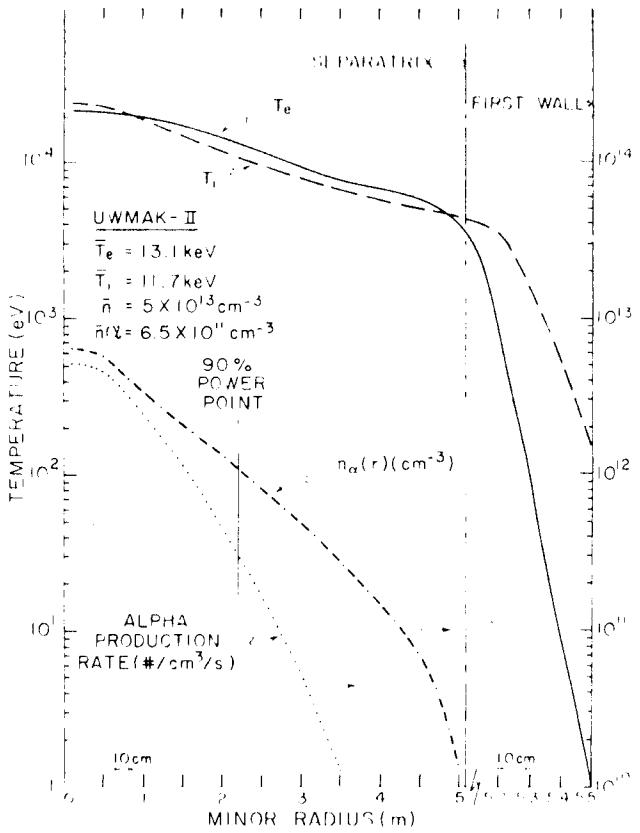

Fig.14 Profiles of temperature and alpha production at steady state in UWMAK-II.

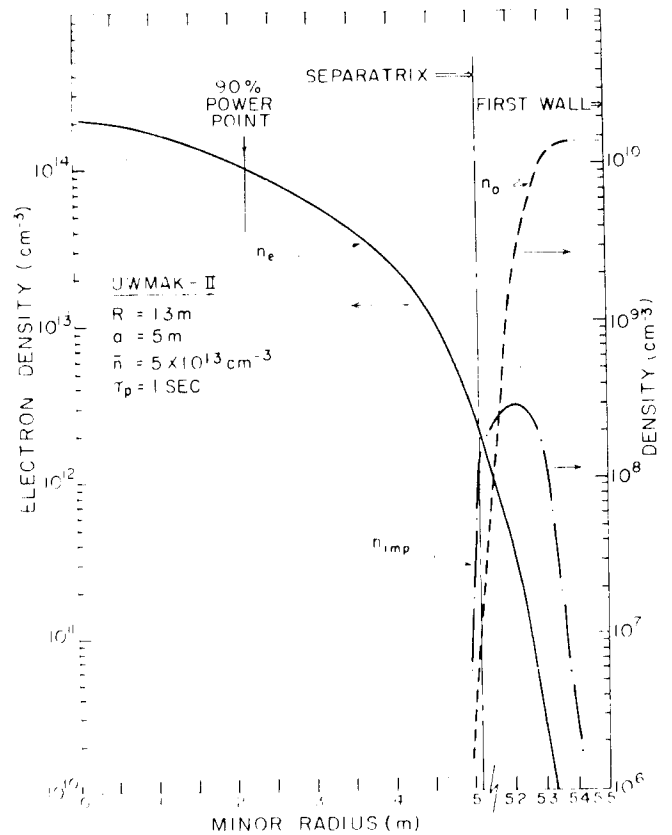

Fig.15 Profiles of the electron, impurity and neutral densities at steady state in UWMAK-II.

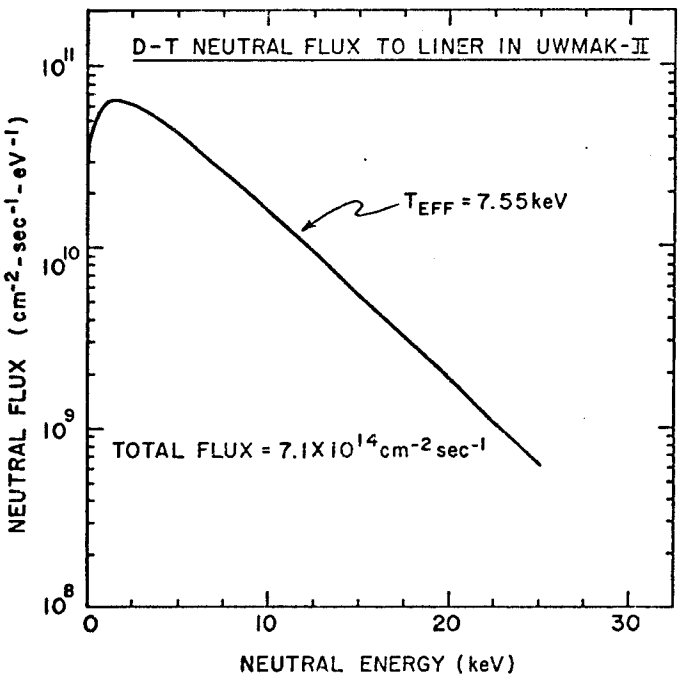

Fig.16 Neutral D-T flux to the liner at steady state in UWMAK-II.

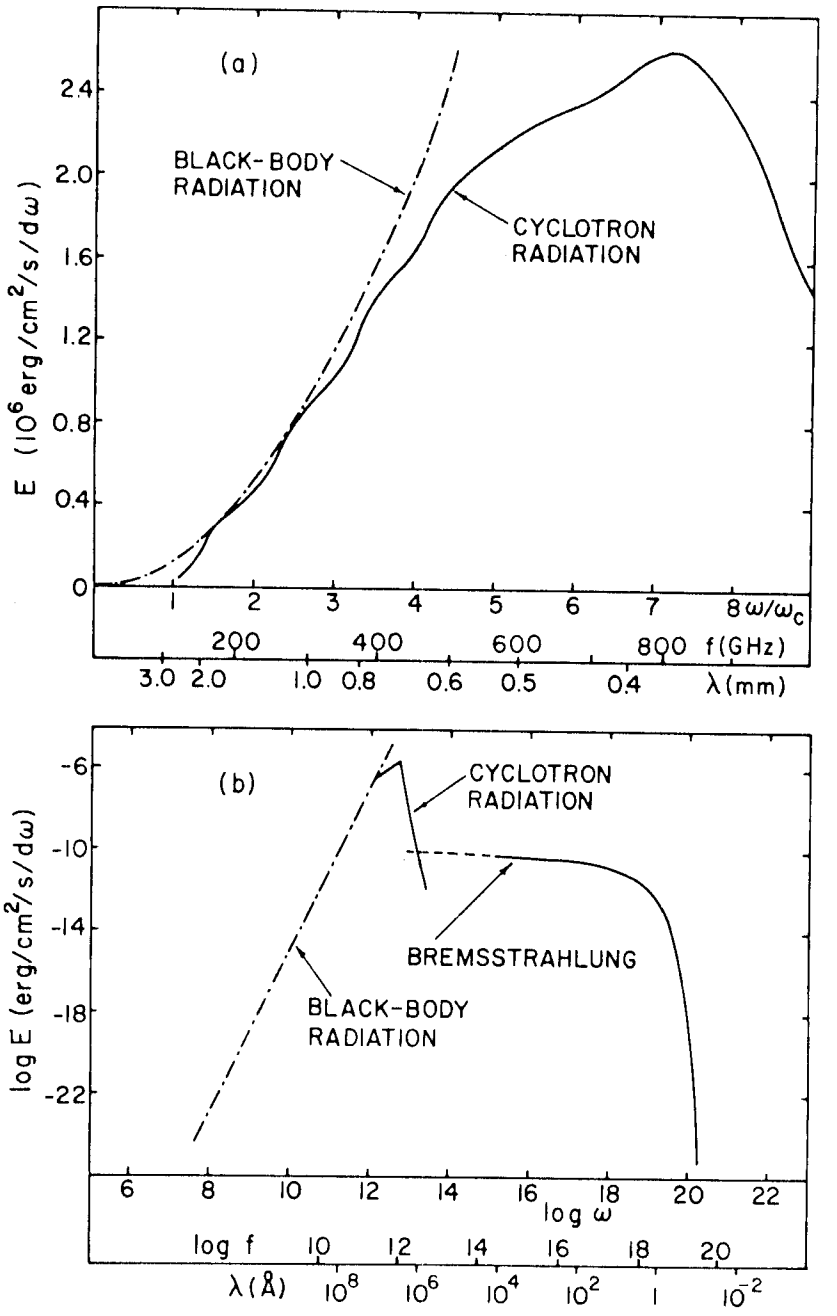

Fig. 17 - The spectrum of cyclotron and bremsstrahlung radiation emitted by a thermonuclear tokamak plasma at 10 keV. At low frequency, cyclotron emission dominates bremsstrahlung but the bremsstrahlung spectrum is is white up to $\omega \sim 10^{20}$ rad/sec.

Plasma contamination by impurities is detrimental for several reasons. First, impurities cause excessive radiation losses which makes the achievement of ignition conditions more difficult [5,6]. Second, they cause an increase in the effective Z of the plasma which can distort temperature and density profiles and can lead to a more rapid attenuation of injected neutral beams [7]. Finally, the slow buildup of impurities can limit the burn time achievable in tokamak reactors [6].

2. Modeling of Tokamak Plasmas

Tokamak plasma modeling involves the solution of the space and time dependent particle continuity and energy conservation equations self consistently with the solution of Maxwell's equations and the transport of neutral atoms [9]. The elements included in such models can be understood by examining Fig. 1. Hydrogenic ions, impurities and electrons interact via rethermalization while neutral beam injection or fusion alpha particles slow down and heat the various species. Neutral gas surrounding the plasma can enter and interact via charge exchange with the hydrogenic ions. Electrons can gain energy from ohmic heating and each species losses both particles and energy by various processes that include conduction, convection, unconfined particle banana orbits, radiation, and charge exchange of cold neutrals with hot ions.

Ions and electrons diffusing from the plasma interact with the limiter or are collected using a magnetic divertor [10]. This can give rise to desorption and backstreaming of neutrals as well as evaporation and sputtering at the limiter. Neutral particles, electromagnetic radiation and neutrons interact primarily with the vacuum chamber liner or first wall and cause desorption and sputtering of the liner as well as desorption and reflection of hydrogenic neutrals.

Two numerical models have been used to carry out the analysis reported in this paper. The first is a one dimensional space-time fluid model in which the plasma radius is the primary spatial coordinate and cylindrical symmetry is assumed. The equations are:

$$\frac{\partial n_i}{\partial t} = \frac{1}{r}\frac{\partial}{\partial r}\left(rD\frac{\partial n_i}{\partial r}\right); \quad n_e = n_i + 2n_\alpha + \sum_j n_{z_j} Z_j; \qquad (1)$$

$$\frac{\partial n_i T_i}{\partial t} = -4.28 \times 10^{-11} n_i n_e \frac{(T_i - T_e)}{T_e^{3/2}} + \frac{2}{3r}\frac{\partial}{\partial r}\left(r n_i \chi_i \frac{\partial T_i}{\partial r}\right) - \frac{1}{r}\frac{\partial}{\partial r}(r n_i V_i T_i)$$

$$+ 4.17 \times 10^{15} \{n_D n_T \langle\sigma v\rangle_{DT} U_{\alpha i} P_{ex} + P_{inj}(U_{bi} + f(\frac{E_\alpha}{E_B})U_{\alpha i})\} \qquad (2)$$

$$\frac{\partial n_e T_e}{\partial t} = 4.28 \times 10^{-11} n_e n_i \frac{(T_i - T_e)}{T_e^{3/2}} + \frac{2}{3r}\frac{\partial}{\partial r}\left(r n_e \chi_e \frac{\partial T_e}{\partial r}\right) - \frac{1}{r}\frac{\partial}{\partial r}(r n_e V_e T_e)$$

$$+ 4.17 \times 10^{15} \{n_D n_T \langle\sigma v\rangle U_{\alpha e} + \underline{E} \cdot \underline{J} + P_{inj}(U_{be} + f(\frac{E_\alpha}{E_b}) U_{\alpha e}) - P_B - P_S - P_L - P_R\} \qquad (3)$$

$$\frac{\partial B_\theta}{\partial t} = 10^5 \times \frac{\partial E}{\partial r} \quad ; \quad \frac{\partial J}{\partial t} = 7.96 \times 10^4 \frac{1}{r}\frac{\partial}{\partial r}\left(r \frac{\partial E}{\partial r}\right); \quad E = \eta_{NC} J \quad . \qquad (4\text{-}6)$$

$T_{e,(i)}$ is the electron (ion) temperature (eV), B_θ is the poloidal magnetic field (gauss), $n_{e,(i)}$ is the electron (ion) density (cm^{-3}), V_i is the ion velocity (cm/ms), J is the toroidal current density (amp/cm^2), E is the toroidal electric field (volt/cm), r is the radius (cm), t is time (ms), $\chi_{e,(i)}$ is the electron (ion) thermal diffusivity (cm^2/ms), η_{NC} is the neoclassical resistivity (ohm-cm), D is the diffusion coefficient (cm^2/ms), $U_{bi,(e)}$ is the fraction of beam energy going to ions (electrons), $U_{\alpha i,(e)}$ is the fraction of alpha energy going to ions (electrons), and f is the fraction of deuterons (tritons) in the neutral beam which undergo fusion as they slow down in the target plasma. P_B, P_S, P_L, and P_R represent bremsstrahlung, synchrotron, line and recombination radiation, respectively (watts), P_{cx} is the energy loss due to charge exchange (watts), and S is the source of ($cm^{-3}ms^{-1}$) due to a cold plasma or neutral particle reflux. These equations must be solved subject to appropriate boundary conditions at the plasma edge or to a self consistent matching of the main plasma with the region near the first wall.

The second more simplified model is to employ prescribed spatial profiles for the plasma density, temperature, and current and thereby reduce the equations to a set of ordinary first order differential equations in time. These can be solved quite inexpensively and in this way, one can follow the time evolution of the average plasma parameters. It is still possible to estimate wall fluxes of, for example, neutral particles by evaluating the neutral reflux to the plasma at a given time and carrying out the space dependent neutral transport calcula-

tion. This will give the spectrum of neutral particles leaving the plasma and allow us to estimate the effects of first wall interaction phenomena.

3. Data Requirements for Tokamak Plasma Modeling

There are three major categories where input information is required for the plasma models described in the previous section. The first is plasma transport coefficients, mainly the thermal conductivity and diffusion coefficients for ions and electrons. The second is atomic physics data characterizing radiation processes in the plasma, such as ionization and recombination coefficients, and oscillator strengths, and processes that will effect the trapping of neutral beams such as the trapping of deuterons on multiply charge ions. The third is surface physics data including such quantities as photodesorption rates, hydrogenic sputtering yields, self sputtering yields, neutral particle reflection coefficients and energy spectra, and charged to neutral ratios of backscattered particles.

Considering the plasma physics input, the modeling of plasmas in reactor systems requires the knowledge of transport coefficients in regimes of plasma temperature and density that have not yet been achieved experimentally. It should be clear therefore that estimates of fluxes to the walls of future devices are inherently uncertain and, while we report such quantities as a guide to surface physicists, these uncertainties should be kept in mind.

To illustrate this problem, the perpendicular diffusion coefficient is plotted in Fig. 2 as a function of reduced collision frequency, ν_{eff}/ω_{be}, from predictions of various theories. Here, $\nu_{eff} = A\,\nu_{ei}$, ν_{ei} is the electron ion collision frequency, A is the aspect ratio, and ω_{be} is the bounce frequency of electrons trapped in the toroidal field. Thermonuclear plasmas are expected to operate at low collision frequencies, in the trapped ion regime on the figure. One can see that the predictions of classical theory [11], neoclassical theory [12], and trapped particle microinstability theory [13] differ substantially in the low collisionality regime. Clearly, microinstability theory predicts much more rapid diffusion (and thus much shorter particle confinement times) than does classical or neoclassical theory. Just as clearly, calculations of plasma behavior and first wall fluxes can differ markedly depending on the transport theory assumed. Present day experiments appear to follow pseudoclassical theory with the hottest plasmas just beginning to enter the trapped electron regime of collisionality. On the other hand, high density tokamak plasmas such as in the Alcator machine

[14] do not follow pseudoclassical predications but rather give an overall energy confinement times that is proportional to the density but does not depend on temperature. In the calculations reported here, the theoretical predictions of microinstability theory [13] in a form analogous to the "six regime" model [15, 16] have been used. The estimated transport coefficients are admittedly order-of-magnitude but the assumption is that such rapid diffusion can only provide a pessimisstic model.

Surface physics data is required to successfully model tokamak plasmas and this data is rapidly being generated [1]. Nevertheless, much work remains and these requirements are illustrated briefly by discussing two specific phenomena, sputtering and reflection. Sputtering yield data for various species incident on stainless steel is summarized in Fig. 3 as complied by Behrisch [1]. One can see the sparity of data below 1 keV and the difference between the recent data at 500 eV and an earlier fit suggested by Meade et al. [15]. In the important range from threshold to 1 keV, various extrapolations can readily differ by an order of magnitude. Further, the data for D^+ on stainless steel is much higher than the data for incident H^+ while one would expect the sputtering yields to differ by the ratio of the masses, namely 2 to 1. This latter fact clearly needs to be established experimentally. The extensive study by Finfgeld [17], whose data is summarized in Table 1, does indicate that $S(D^+)/S(H^+)$ is about 2 in the 1-10 keV range.

Carbon in various forms has been suggested as a low Z liner for tokamaks to avoid the large radiative losses caused by high Z impurities [18, 19, 1]. Sputtering yield measurements are summarized in Fig. 4 and one again notes the absence of data below 1 keV. In the calculations to be discussed, a fit indicated by the dashed lines in Figs. 3 and 4 has been used to model the sputtering yields. These fits were multiplied by the appropriate mass artio to model sputtering by a 50-50 D-T plasma or a pure tritium plasma.

Another important quantity required is the refelction coefficient for high energy neutrals incident on various surfaces and experiments are beginning in this area [20]. The theoretical results of Oen and Robinson [21] shown in Fig. 5 have been used for both the reflection coefficient and the energy distirbution of reflected particles.

4. A Small Two Component Tokamak

A two component tokamak (TCT) is a device in which a high energy deuterium neutral beam, typically with an energy exceeding 120 keV, is injected into a pure tritium target plasma. When the electron temperature exceeds about 4.5 keV, the energy released in beam-plasma fusion reactions can approximately reproduce the energy injected into the target plasma [8]. Furthermore, this energy breakeven can be achieved at an $n\tau_E$ value of about 10^{13} cm^{-3}-s^{-1} and the operation of a tokamak in this manner is the optimum way to generate a high 14 MeV neutron flux [22]. For these reasons, such a device is of interest in the near term as a fusion test reactor [2], as a materials and engineering test reactor [23], and as a hybrid reactor. The anticipated plasma performance and wall fluxes in such a device are therefore of considerable interest.

Typical parameters for a relatively small TCT are listed in table 2. The neutral beam is assumed to be produced from a positive ion source which has D^+, D_2^+, and D_3^+ components [24]. The source composition is taken as 75% D^+, 15% D_2^+, and 10% D_3^+. Assuming neutralization efficiencies [25] of 33% for D^+, 65% for D_2^+ and 78% for D_3^+, the fraction of the 40 MW that is injected as atomic and molecular species is indicated in Table 2. This is important because the D_2° and D_3° components have 75 keV and 50 keV per deuteron, respectively, and are not as penetrating. Further, the cross section for charge exchange is larger at these low energies such that there is a greater probability of these beam injected ions charge exchanging near the plasma edge and giving rise to fast neutrals.
In these calculations, the neutral particle outflux from both beam charge exchange and from the transport of initially low energy recycle neutrals are included. (Note that if negative ion sources can be successfully operated at these power levels, they would produce only the primary neutral at, e.g., 150 keV.)

The burn cycle scenario that has been analyzed assumes the plasma has been set up at full operating current and has reached a temperature of about 1 keV. Time zero is defined as the time when the 40 MW of neutral beam injection is turned on.

Two types of liners have been considered, stainless steel (iron) and carbon and the plasma density and temperature profiles are taken to be parabolic.

The boundary condition on temperature at the plasma edge is 10 eV, based on the assumption that the Franck-Condon process produces a 5-10 eV neutral at the plasma boundary. The 10 eV boundary condition appears to be supported by recent temperature profile measurements in the TFR machine [26]. The plasma density is maintained by a recycle boundary condition in which T_2 molecules are recycled into the plasma and ionized via the Franck-Condon process at a rate sufficient to make up for losses due to plasma diffusion.

At specified times, the neutrals recycled as well as the neutrals from charge exchange on the beam are transported in space using a linear Boltzmann equation. The neutral outflux to the liner is calculated and the reflection and sputtering is evaluated. The reflected particles are again transported and the calculational cycle is repeated until convergence is achieved. (Convergence is fairly rapid because the reflection coefficient is typically less than 0.5.) The sputtered impurity atoms enter the plasma and, as a worse case, are assumed to accumulate. This is somewhat equivalent to assuming that impurities diffusing from the plasma strike the limiter with a self sputtering coefficient of one. (This also assumes the liner and limiter are made of the same material.) Finally, plasma ions diffusing from the plasma at a temperature of about 10 eV do not cause sputtering of the limiter. As such, these particles are taken to be neutralized and to become part of the gas participating in the recycle process.

The electron and ion temperatures and the impurity concentration are shown as a function of time in Fig. 6 for the case of a stainless steel liner. The initial impurity content is taken to be 0.1%. The average electron temperature reaches a maximum at about 300 ms and then begins to drop rapidly because of the excessive radiation losses as the iron enters the plasma. This clearly demonstrates the importance of wall interactions <u>even if</u> the plasma starts out relatively clean.

Neutral sputtering of the liner is the cause of the impurity influx. These neutrals come from two sources, charge exchange associated with recycled neutrals and charge exchange of the injected beam particles. The neutral beam deposition profile in the plasma is shown in Fig. 7 and one notes that the half

and third energy components are deposited mostly near the plasma edge. The charge exchange neutral flux to the liner is shown in Fig. 8 and 9 at 100 ms and 300 ms, respectively. At early times when the particle confinement time, τ_p, is long (~1 sec), the neutral outflux due to charge exchange trapping of the injected beam is about equal in magnitude to that associated with recycle. However, the neutrals from beam charge exchange have a much hotter energy distribution and a relatively long high energy tail. At 300 ms, the plasma has entered the trapped particle regime and τ_p has dropped. The recycle flux therefore increases and has a higher effective temperature.

The variation of the temperature and impurity concentration with time in the low Z, carbon liner case is shown in Fig. 10. The initial carbon content was assumed to be 1%. The carbon buildup is substantial but the effect on plasma temperature is minimal. Note however that the plasma amplification factor, Q, as defined in [8], does begin to decrease. The reason is the build-up of plasma density due to beam injection. The calculated total neutral flux to the liner is given in Fig. 11 as a function of time. The levels in both cases are 1-2 x 10^{15} neutrals/cm^2sec.

Alpha particle bombardment of the liner in two component devices can be important because the alpha production profile is relatively broad and the plasma current is typically low. As such, some alpha particles born at 3.52 MeV are on trapped orbits which extend outside the plasma radius and can intersect the wall [27].

The radial profile of alpha production from beam plasma fusions is shown in Fig. 12. Alpha particles born with their velocity vector, $\underline{v}$, such that $\underline{v} \cdot \underline{J}p < 0$, where $\underline{J}p$ is the vector plasma current, are referred to as counter-streaming particles and are least well confined. The fraction of counter-streaming alphas with orbits extending outside the plasma radius, a = 1m, is also shown in Fig. 12 as a function of the reduced minor radius, r/a. All counterstreaming alphas born within 20% of the plasma edge are lost. The overall situation is summarized in Table 3. Assuming the liner is at the plasma boundary, 21% of the alpha particles born at 3.5 MeV strike the liner. The average 3.5 MeV alpha flux at r = a is 7.5 x 10^{11} cm^{-2}-s^{-1} and local values can be higher. Of course, this flux can be reduced by moving

the wall away from the plasma edge by 10-20 cm but this increases the overall size of the device. Thus, alpha bombardment of the liner in small TCT devices can be a serious problem.

5. Conceptual Tokamak Reactor Analysis

The plasma performance and wall fluxes expected in full scale pure fusion reactors will be illustrated by analysing the UWMAK-II conceptual tokamak reactor [3]. The main plasma parameters are: major radius, 13m; plasma radius, 5m; plasma current, 14.9MA; toroidal magnetic field, 36kG; plasma composition 50%D, 50%T. For impurity control, the plasma has been designed with a double null poloidal field divertor [10] and a low Z carbon liner [18]. A separatrix divides the plasma into a main confinement region and a scrape-off region between the separatrix and the liner, as shown in Fig. 13. Particles on field lines inside the separatrix are confined to the main body of the plasma while particles in the scrape-off region are carried along field lines to the collector plates above and below the null points.

Mense [28] has analysed this plasma at the thermally stable operating point using the space-time equations described in section 2 to model the plasma within the separatrix. In addition, plasma transport in the scrape-off layer is also modeled.

Cross field transport plus streaming along field lines to the collector plates means that transport in the scrape-off region is inherently two dimensional. The problem is converted to one dimension by approximating the parallel particle flux, $\nabla \cdot \vec{\Gamma}_{//}$, by $\Gamma_{//}/L(r)$ and the parallel heat flux, $\nabla \cdot \vec{Q}_{//}$ by $Q_{//}/L(r)$. $L(r)$ represents the average distance along a field line to the collector plates starting at the plasma midplane. $\Gamma_{//}$ is determined by requiring that the net electrical current traveling along a field line to the collector plate is zero, i.e., $(n_i \vec{V}^i_{//} - N_e \vec{V}^e_{//})e = \vec{J}_{//} = 0$. The electrostatic sheath thus established is evaluated and used to determine the electron parallel heat flow, $Q^e_{//}$. The cross field conduction and convection is taken to follow Bohm scaling because the gradients which develop in the scrape-off region are very steep. In addition, 10% of all plasma particles collected at the divertor plates are refluxed as D_2 or T_2 gas back into the plasma chamber. This is the source of the neutrals which participate in charge exchange. The largest contribution to the charge exchange flux incident on the liner comes from the region near the separatrix.

Sputtered impurity ions are assumed to be ejected isotropically with a mean energy of 20 eV. This energy is perhaps high but is pessimistic in that such impurities have a higher probability of reaching the main confinement region inside the separatrix.

The electron and ion temperature profiles and the alpha particle production rate are shown in Fig. 14 while the electron density and neutral density profiles are shown in Fig. 15. Also shown in Fig. 15 is the ionization profile of neutral impurity atoms sputtered from the liner. One notes first that the temperature profiles are relatively broad but that the electron temperature drops sharply beyond the separatrix. This latter effect is due to the development of the sheath potential at the collector which leads to preferential collection of high energy electrons.

By contrast to the temperature profile, the density profile is very sharp. This means the divertor is essentially 100% effective at collecting particles diffusing from the plasma. The density at the liner is calculated to be less than 10^{-4} of the density at the separatrix which, in turn, is two orders of magnitude below the centerline value. Nevertheless, we note that the density just outside the separatrix is $\sim 10^{12} cm^{-3}$. As such, approximately 95% of the sputtered impurity atoms are ionized outside the separatrix. This indicates that the divertor is effective at both collecting plasma which diffuse across the separatrix and at shielding the plasma from sputtered impurities. If born out experimentally, this would indicate that divertors can be very effective at impurity control.

The sharply peaked alpha particle production profile in this ignited D-T plasma is in contrast to the same quantity in a TCT that is shown in Fig. 11. 90% of the alpha production is now within 40% of the plasma center. At a plasma current of about 15 MA, one would calculate that essentially no 3.5 MeV alpha particles strike the liner. This will be true even if toroidal field ripple trapping [3,29] is considered because the alpha birth profile is so sharply peaked. Thus, one expects the alpha particles diffusing from a large, ignited tokamak plasma to do so at essentially the same temperature as the fuel ions. Further, since the alpha particle is doubly charged, any charge exchange neutral helium flux to the liner will be negligibly small.

The hydrogenic neutral reflux from the divertor collectors gives rise to a neutral D-T flux to the liner as shown in Fig. 16. The energy spectrum reflects the fact that the ion temperature near the separatrix is approximately 5 keV. This temperature is coincidentally near the peak of the sputtering yield curves in Figs. 3 and 4.

6. Spectrum of Synchrotron and Bremsstrahlung Radiation

Radiation will be emitted from plasmas due to bound-bound transitions or line radiation, free-bound or bound-free transitions, bremsstrahlung, and synchrotron radiation. At electron temperatures below about 10 keV, high Z impurities like Fe are not fully stripped. In this case, line and recombination radiation will dominate radiative losses and the spectrum emitted will depend on the impurity element. In ignited D-T plasmas operating at temperatures above 10 keV, bremsstrahlung and synchrotron radiation will begin to dominate. We have calculated the spectrum of such radiation for a characteristic tokamak reactor system that is somewhat smaller in size than UWMAK-II. For this characteristic machine, the parameters are: plasma radius, 2.5m; first wall radius, 2.75m; aspect ratio, 3; toroidal magnetic field on axis, 40 kG. These parameters are more characteristic of a smaller near term tokamak reactor of lower power output than UWMAK-II. The calculations were done in cylindrical coordinates rather than assuming the plasma is a slab, as has been done in previous calculations. The toroidal field is assumed to vary with major radius as 1/R across the cylinder and the electron density and temperature are both assumed to have parabolic profiles across the plasma. The average temperature is 10 keV and the average density is $10^{14}/cm^3/sec$.

The energy deposited per unit of surface area is obtained from the formula of Costley et al., [30] namely,

$$W_s = 2I_{BB}\frac{1-e^{-\tau}}{1-\hat{r}\,e^{-\tau}} \simeq 2I_{BB}\frac{\tau}{(1-\hat{r})+\tau}$$

where I_{BB} is the blackbody intensity [31], τ is the optical depth, and $\hat{r}$ is the effective reflection coefficient (accounting for both material properties and penetrations or holes in the first wall). The optical depth is obtained by integrating the spectral absorptivity along a light path, assumed to be straight. The formulae of Engelmann and Curatolo [32] and Audenaude [33] were used to find the spectral absorptivity. We have used $\hat{r}$ equal to 0.95.

The spectrum of the radiation deposited at a point on the equatorial plane of the torus is shown in Fig. 17. This spectrum will vary with poloidal angle but the results given here may be taken as characteristic of a tokamak fusion

plasma. The synchrotron radiation spectrum given in Fig. 17a shows that at 10 keV, the contribution from various harmonics strongly overlap such that the typical line spectrum at multiples of the electron cyclotron frequency, ω_c^e, has completely disappeared. The harmonics for which the plasma is optically thick, i.e., those for which the curve in Fig. 17a follows the black-body parabola, are still somewhat identifiable. However, for the higher harmonics, the spectrum is completely continuous.

Bremsstrahlung is also included in this analysis but it is unimportant at frequencies where there is appreciable cyclotron emission (see Fig. 17b). However, the total energy emitted due to bremsstrahlung <u>is</u> important because the spectrum is essentially white up to $\omega \simeq \frac{kT_e}{\hbar}$ which is in the range, 10^{19}-10^{20}rad/sec. Thus the integral amount of bremsstrahlung emission is, at 10 keV, of the same order of magnitude as the synchrotron emission and exceeds it at lower temperatures.

The total bremsstrahlung emission from a plasma is given by

$$P_B = 4.8 \times 10^{-31} n_e^2 Z_{eff} T_e^{1/2} (W/cm^3) \quad Z_{eff} = \frac{\sum_j n_j Z_j^2}{n_e} \qquad (7\text{-}8)$$

where the sum extends over all ionic species. A rigorous analytical formula for total synchrotron emission does not exist but an approximate formula given by Yang [34]

$$P_c = 7.2 \times 10^{-13} (1 - 0.013A)^3 \left(\frac{n_e}{qAIp}\right)^{1/2} B_T^3 T_e^{2.1} \ (W/cm^3) \qquad (9)$$

appears reasonable. Here, n_e is in cm^{-3}, T_e is in keV, Ip is in MA, and B_T is in tesla. Equations (7) and (9) can thus be used to estimate the surface radiation loading from a tokamak reactor plasma operating at specified values of electron temperature, density, effective Z, magnetic field strength, and plasma current.

7. Conclusions

Anticipated fluxes of neutral particles to the walls of tokamak reactor devices are in the 10^{15}cm^{-2}-sec^{-1} range and have a spectrum that depends on the plasma temperature profiles, the conditions near the edge, and the characteristics of auxiliary heating systems such as neutral beam injection. Photon fluxes from synchrotron radiation and bremsstrahlung will vary with the size of the device, the electron temperature, and the magnetic field strength. The typical synchrotron spectrum is peaked at about 7 ω_c^e which is typically a low frequency in the 8 x 10^{11} Hz range ($\lambda \sim 0.3$mm). The bremsstrahlung spectrum is much broader, being essentially uniform out to energies near T_e. Thus, most of the bremsstrahlung energy is carried away by photons in the soft x-ray range and for T_e = 10 keV, the maximum frequency is $\sim 10^{18}$Hz ($\lambda \sim 1.0$ Å).

The plasma modeling programs that are used to assess plasma performance and to generate results such as those presented in this paper require plasma transport coefficients, atomic physics data, and surface physics data. The most important surface physics data requirements include: sputtering yields for incident hydrogen in the 10eV-10keV range on various samples of pure materials and alloys; relative sputtering yields for H, D, and T over the same incident energy range; angle and energy dependent reflection coefficients; energy distribution of reflected particles; ion to neutral ratios in backscattering; chemical effects on surface yields under hydrogenic bombardment as a function of temperature, particularly for materials like carbon; photodesorption yields; and erosion rates of surfaces under high energy helium bombardment. Improved data in these areas will help in the development of a more complete treatment of the plasma boundary problem. Atomic physics data is needed to improve our treatment of radiative losses and impurity behavior in plasmas. It is also important to measure cross sections for the trapping of neutral deuterons on multicharged ions to properly assess the impact of impurities on enhanced beam trapping. However, the area of greatest uncertainty at present remains in the plasma physics itself, particularly in the knowledge of transport coefficients. For this, the greatest need is for larger tokamak experiments to provide new experimental information that can guide us towards a fuller understanding of tokamak plasmas.

Acknowledgment: The authors thank Dr. D. G. McAlees for the TCT alpha particle calculations and Dr. K. Audenaerde for help in computing the synchrotron radiation spectrum. This research was supported by grants from the Wisconsin Electric Utility Research Foundation and the U.S. Energy Research and Development Administration.

REFERENCES

[1] R. Behrisch and B. B. Kadomtsev, in Plasma Physics and Controlled Nuclear Fusion Research 1974 (IAEA, Vienna, 1975) Vol. II, p. 229.

[2] Two Component Torus, Joint Conceptual Design Study (Princeton Plasma Physics Laboratory and Westinghouse Electric Corp., June, 1974) Vols. I, II, III.

[3] R. W. Conn et al., in Plasma Physics and Controlled Nuclear Fusion Research 1974 (IAEA, Vienna, 1975) Vol. III, p. 497. Also, B. Badger et al. "UWMAK-II, A Conceptual D-T Fueled, Helium Cooled, Tokamak Fusion Power Reactor Design, Nucl. Eng. Dept. Report UWFDM-112 (Univ. of Wisconsin, Dec. 1975).

[4] O. K. Harling, M. T. Thomas, R. L. Broadzinski, L. A. Rancitelli, Trans. Amer. Nucl. Soc. 22 (1975) 35.

[5] D. Meade, Nucl. Fus. 14 (1974) 289.

[6] R. W. Conn and J. Kesner, Nucl. Fus. 15 (1975) 775.

[7] J. P. Girard, D. Marty, P. Moriette, in Plasma Physics & Controlled Nuclear Fusion Research (IAEA, Vienna, 1975) Vol. I, p. 681.

[8] J. Dawson, H. P. Furth, F. Tenney, Phys. Rev. Letts. 26 (1971) 1156.

[9] J. Hogan, Meth. in Comp. Physics 16. (1976). Also, Oak Ridge National Lab. Rept. ORNL-TM-5153 (1975).

[10] G. A. Emmert, J. M. Donhowe, A. T. Mense, J. Nucl. Mat. 53 (1974) 39.

[11] L. Spitzer, The Physics of Fully Ionized Gases (Interscience, New York, 1967).

[12] M. N. Rosenbluth, R. Hazeltine, F. L. Hinton, Phys. Flds. 15 (1972)116.

[13] B. B. Kadomtsev, O. P. Pogutse, in Reviews of Plasma Physics (M. A. Leontovich, ed., Consultants Bureau New York) Vol. 5 (1970). Also, Sov. Phys - JETP 24 1172 (1967) and Sov. Phys.-Dokl. 14, 470 (1969).

[14] D. S. Pappas, J. deVilliers, H Helava, R. R. Parker, R. J. Taylor, "Alcator Scaling Laws" Bull. Amer. Phys. Soc. 20,1360(1975).

[15] D. Meade, H. Furth, P. H. Rutherford, F. Seidl, D. Duchs in Plasma Physics and Controlled Fusion Research 1974 (IAEA, Vienna, 1975) Vol.I, p. 605.

[16] S. O. Dean et al. "Status and Objectives of Tokamak Systems for Fusion Research," USAEC Report, WASH-1295 (1974).

[17] C. R. Finfgeld, "Proton Sputtering" U.S.A.E.C. Final Report, ORO-3557-15 (1975).

[18] G. L. Kulcinski, R. W. Conn, G. Lang, Nucl. Fus. 15 (1975) 327.

[19] G. Hopkins, in Plasma Physics and Controlled Nuclear Fusion Research 1974 (IAEA,Vienna, 1975) Vol. II, p. 275.

[20] R. Behrisch, W. Eckstein, P. Meischer, B. M. U. Scherzer, H. Verbeek, in Atomic Collision Phenomena in Solids, S. Datz et al., eds. (Plenum Pub. Corp., New York, 1975.) Vol. 1, p. 315. Also, W. Eckstein, H. Verbeek, P. Matsche, J. Nucl. Mat. (this issue)

[21] O. Oen, M. T. Robinson, J. Nucl. Mat. (this issue)

[22] D. L. Jassby, Nucl. Fus. 15 (1975) 453.

[23] R. W. Conn, D. L. Jassby, "A Tokamak Engineering Test Reactor," Princeton Plasma Physics Lab. Report, MATT-1155 (Aug. 1975).

[24] J. H. Fink, W. L. Barr, G. W. Hamilton, Nucl. Fus. 15 (1975) 1067.

[25] K. H. Berkner, R. Pyle, J. Stearns, in Proc. First Nat'l Top. Conf. on The Technology of Controlled Nuclear Fusion (Conf-740402-P1, USAEC, 1974) Vol. 1, p. 432.

[26] P. Ginot, TFR Group, J. Nucl. Mat. (this issue).

[27] D. G. McAlees, "Alpha Particle Energetics and Neutral Beam Heating in Tokamak Plasmas," Ph.D. Thesis, University of Wisconsin (1974).

[28] A. T. Mense," Poloidal Divertors for Tokamak Reactors," Ph.D. Thesis, University of Wisconsin (1976).

[29] T. F. Yang, G. A. Emmert, in Proc. First National Top. Conf. on the Tech. of Controlled Nucl. Fusion (CONF-740402-P2, USAEC, 1974) Vol. 2, p. 400.

[30] A. E. Costley, R. J. Hastie, J. W. M. Paul, J. Chamberlain, Phys. Rev. Letts. 33 (1974) 758.

[31] G. Bekefi, Radiation Processes in Plasmas (J. Wiley and Sons, Inc., New York, N. Y., 1966).

[32] F. Engelmann, M. Curatolo, Nucl. Fus. 13 (1973) 497.

[33] K. Audenaerde, "Cyclotron Emission from a Dense Plasma," Ph.D. Thesis, R. U. Utrecht (1976).

[34] T. F. Yang, G. A. Emmert, H. Forsen, "The Calculation and Parametric Study of Synchrotron Radiation Loss for Tokamak Reactors" Nuclear Eng. Dept. Report FDM-49, University of Wisconsin (1973).